Nanoscale

Accepted Manuscript

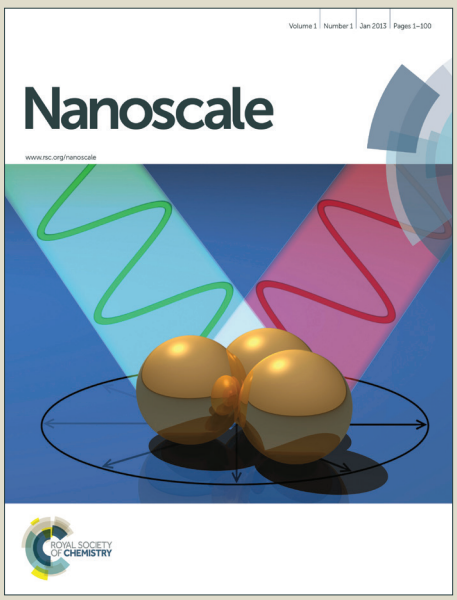

ROYAL SOCIETY OF CHEMISTRY

www.rsc.org/nanoscale

Journal Name

RSCPublishing

ARTICLE

Adsorbent 2D and 3D Carbon Matrices with Protected Magnetic Iron Nanoparticles

Cite this: DOI: 10.1039/x0xx00000x

N. L. V. Carreño,[a] M. Escote,[b] A. Valentini,[c] L. McCafferty,[d] V. Stolojan,[d] M. Beliatis,[d] C. A. Mills,[d,e] R. Rhodes,[d] C. T. G. Smith,[d] and S. R. P. Silva[d]

Received 00th January 2012,
Accepted 00th January 2012

DOI: 10.1039/x0xx00000x

www.rsc.org/

We report on the synthesis of two and three dimensional carbonaceous sponges produced directly from graphene oxide (GO) into which functionalized iron nanoparticles can be introduced to render it magnetic. This simple, low cost procedure, wherein an iron polymeric resin precursor is introduced into the carbon framework, results in carbon-based materials with specific surface areas of the order of 93 and 66 m^2/g, compared to approx. 4 m^2/g for graphite, decorated with ferromagnetic iron nanoparticles giving coercivity fields postulated to be 216 and 98 kG, values typical for ferrite magnets, for 3.2 and 13.5 wt. % Fe respectively. The strongly magnetic iron nanoparticles are robustly anchored to the GO sheets by a layer of residual graphite, on the order of 5 nm, formed during the pyrolysis of the precursor material. The applicability of the carbon sponges is demonstrated in their ability to absorb, store and subsequently elute an organic dye, Rhodamine B, from water as required. It is possible to regenerate the carbon-iron hybrid material after adsorption by eluting the dye with a solvent to which it has a high affinity, such as ethanol. The use of a carbon framework opens the hybrid materials to further chemical functionalization, for enhanced chemical uptake of contaminants, or co-decoration with, for example, silver nanoparticles for bactericidal properties. Such analytical properties, combined with the material's magnetic character, offer solutions for environmental decontamination at land and sea, wastewater purification, solvent extraction, and for the concentration of dilute species.

1 Introduction

Chemical spills, be they of organic materials, such as oil, heavy metals, or other contaminants, require an immediate response in order to mitigate irreversible economic and ecological damage. Such effects can be severe and far reaching; the Deepwater Horizon oil spill, for example, devastated tourism and fishing industries in the Gulf of Mexico, resulting in long-term damages that are measured in the tens of billions of US$. The damage to the ecosystem has been no less serious, with over 650 miles of coastline becoming 'oiled' and mass casualties amongst marine species including the sea turtle [1].

Amongst human communities, the effects on public health are also a concern. In the wake of severe spills, there have been increased levels of physical and psychological sickness due, respectively, to the exposure to toxic material and the severe disruption to daily life that a spill represents. It is well known that heavy metal ions, crude oil, pesticides and other chemical agents are highly toxic [2], often carcinogenic [3] and can cause widespread poisoning through a variety of routes, including inhalation, skin contact, and the ingestion of contaminated flora and fauna.

In order to mitigate future disasters on the scale of Deepwater Horizon, it is necessary to develop effective containment strategies in order to capture oil while still in the ocean, preferably close to the point of release, and prevent it from making landfall. Such strategies would depend upon the development of materials possessing a large surface area and a high affinity for organic compounds [4], a task for which graphene (and its chemically modified derivatives) are an attractive choice. For example, graphene oxide (GO) is useful for a broad range of applications [5], from protective coatings [6] to fuel cells [7] and optoelectronics [8-10] to name but a few, but recent investigations by Bi et al [11] have shown that GO sponges will aggressively remove organic compounds (i.e. octane, diesel, chloroform) from water. Meanwhile, Zhao et al [12] have demonstrated that similar materials, when modified with sulfonate groups, function as a highly efficient adsorbent for heavy metal ions in dispersion. These results indicate that GO-based materials show great promise as carbon filters, and the ability to modify the surface with chemical groups raises the possibility of selective recovery of precious materials from waste solutions [11-15]; its subsequent regeneration further

contributing to the full use of valuable materials during its life cycle.

Unfortunately, while GO is a highly adaptable and hydrophilic material, these same qualities make it difficult to recapture and separate from water in large-scale environments (such as the open ocean), potentially resulting in a situation where the level of contamination is actually increased. As a result, it is necessary to develop a material that possesses the characteristics outlined above (i.e. high surface area and affinity for organic molecules) but also one that can be easily controlled and removed from the solvent media upon the completion of its task.

In this study, we have developed an alternative method to reduce and modify GO sheets, in order to assemble them into magnetic reduced graphene oxide (rGO) sponges with a high affinity and capacity for organic molecules. Iron (Fe) nanoparticles with strong magnetic properties are robustly anchored to the GO sheets by a layer of residual graphite, formed during the pyrolysis of the precursor materials. They show excellent adsorption and desorption properties for organic contaminants such as dyes, and can be shown to be repeatedly used without obvious structural or performance degradation.

Production of the hybrid nanomaterials is achieved using readily obtainable reactants in a simple, low cost procedure, where the nanoengineered ferromagnetic nanoparticles decorate the 2D flakes or 3D sponge materials, and simultaneously the carbon forms a protective graphitic layer over the nanoparticles. The intimate nature of the encapsulation of the nanoparticles by the graphitic carbon is expected to protect the iron from external chemical or environmental effects, allowing for the retention of the magnetic character of the nanomaterials even in extreme environments, and allowing for magnetic manipulation of the hybrid materials. The production of a hybrid system allows us to take advantage of the properties of both the carbon and iron nanomaterials and tailor those properties towards the specific application of water decontamination.

2 Experimental

2.1 GO synthesis

Graphene oxide was prepared via the Hummers and Offeman process [16]. In brief, graphite powder (1 g) was added to concentrated sulphuric acid (H_2SO_4, 23 mL) under stirring and cooled to 0 ^oC via an ice bath. To this sodium nitrate ($NaNO_3$, 0.5 g) was added, followed by the careful addition of potassium permanganate ($KMnO_4$, 3 g). During this exothermic step, the rate of addition was adjusted in order to maintain the temperature below 20 ^oC. After addition, the ice bath was removed and the reaction allowed to stir for 30 min. in ambient conditions, before the addition of deionized water (46 mL) prompted a sharp increase in temperature to around 98 ^oC. After a further 15 minutes, the reaction was terminated through the addition of excess deionized water (140 mL) and hydrogen peroxide solution (H_2O_2, 30 %, 10 mL). The precipitate produced was separated and washed repeatedly via centrifugation with deionized water, before being dried under vacuum at 50 ^oC.

2.2 Fe resin precursor and Fe-rGO powder

The graphene oxide was further modified via the reduction of a polymeric Fe precursor to incorporate metallic Fe-graphite core-shell nanoparticles into the structure, using a method similar to that achieved for decorating carbon nanotubes. [17] The preparation procedure is illustrated in **Scheme 1**. The polymeric precursor (Scheme 1, **B**) was obtained via the dissolution of citric acid (**A**) (CA, Aldrich Chemical Company, USA) and Fe(III) nitrate (using a CA:Fe molar ratio of 6:1) in a mixture of MilliQ water and ethylene glycol (EG) (the amount of ethylene glycol being a 20:80 mass ratio in relation to the CA) [18]. To this, GO flakes (0.4 g) were added and the mixture stirred at 80 ^oC for 1 h. to give a homogeneous mixture (**C**). The GO flakes were retrieved via filtration and dried under vacuum at 50 ^oC for 12 h., producing a dark powder. This powder was subsequently calcined at 750 ^oC for 2 h. under a nitrogen (N_2) atmosphere, producing a powder material (**D**) that was shown to be highly responsive to magnetic fields post processing of the material.

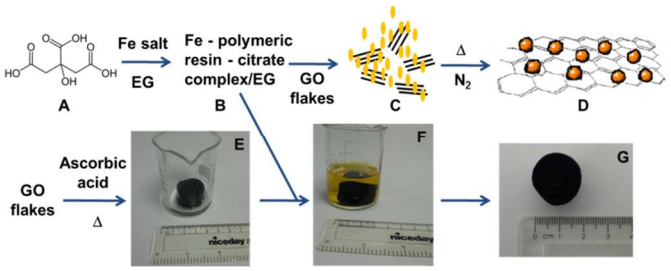

Scheme 1. Production of Fe decorated GO in 2D (D) and 3D (G) conformations, as described in sections 2.2-2.4.

2.3 PDMS immobilized Fe-rGO

Poly(dimethylsiloxane) (PDMS, Sylgard® 184 Silicone Elastomer) polymer nanocomposite was prepared at a ratio of 10:1 (base polymer: cross-linker) to which the Fe-rGO ethanol solution (8 g in 10 mL) was added at the appropriate volume (1 mL) and dispersed via vortex mixing and ultrasonication. The quality of the product was tested for its structural and mechanical integrity using SEM and chemical resistance to high pH levels.

2.4 Fe-rGO sponge synthesis

To prepare the GO sponges, GO was dispersed in water at a concentration of 4 mg/mL. To this, ascorbic acid was added at a 3:1 ascorbic acid:GO mass ratio (i.e. 12 and 4 mg respectively) and the sample sonicated uniformly. The solution was then placed in a sealed vessel and heated at 90 ^oC for 1.5 h. to produce a sponge (Scheme 1, **E**) in a method similar to that described previously. [19] To this, the Fe-polymeric resin citrate complex was added (**F**). The GO sponge was carefully dried under vacuum at 40 ^oC for 6 h., resulting in a reduction in the size of the material (**G**). Once dried, the sponge was heated

at 750 °C for 2 h. under a N_2 atmosphere to create a magnetic material.

2.5 Characterization

The crystalline phases of samples of Fe-rGO were determined by X-ray diffractometry (XRD, Panalytical X'Pert Pro) obtained using Cu Kα radiation (k = 1.5406 Å). The Fe content in the rGO samples was determined using Energy Dispersive X-ray Fluorescence (Shimadzu EDX 720). Imaging of the GO derived hybrid system was performed using scanning electron microscopy (SEM, FEI Quanta 200 environmental SEM), and high resolution transmission electron microscopy (HRTEM, Hitachi HD2300A STEM and Philips CM200 TEM).

Magnetic measurements on the Fe-rGO samples were carried out at room temperature using a vibrating sample magnetometer (VSM, Lakeshore 7407, USA), with an external magnetic field ranging from -1 to 1 kG.

X-ray photoelectron spectroscopy (XPS) analysis was carried out using an Omicron XPS system. Samples were drop cast onto silicon substrates and dried on a hot plate at 150 °C for 5 min., before transferring to the ultra-high vacuum (UHV) system. The load-lock system allowed the samples to be subjected to vacuum for a minimum of 4 hours before being introduced to the main chamber. XPS was carried out at a base pressure of less than $1x10^{-8}$ mbar and using a non-monochromated magnesium X-ray source at 15 kV with a current of 20 mA. All high resolution analysis was carried out in constant analyzer energy (CAE) mode (0.1 eV step size, 0.6 s dwell time, 10 sweeps and 20 eV pass energy).

Temperature-programmed hydrogen reduction (H_2-TPR) was used to study the reducibility of the Fe-rGO composites. TPR was carried out from 100-800 °C at 10 °C/min in a quartz reactor with a flowing 8% H_2/N_2 gaseous mixture (30 mL/min). The H_2 consumption was monitored with a thermal conductivity detector (TCD) connected to the reactor outlet.

The dynamic pulse method was used to measure hydrogen uptake in a custom flow system with the TCD, at room temperature. The Fe-rGO composites sample (0.10 - 0.20 g) is initially reduced in situ to 650 °C, in a quartz microreactor. Hydrogen gas in the system was then removed by flowing nitrogen (N_2), at the same temperature (25 °C) for 30 min. The hydrogen chemisorption was then carried out by pulsing an 8% H_2/N_2 gaseous mixture. Specific surface area measurements were conducted using a Quantachrome apparatus.

3. Results and discussion

3.1 Composite characterization

Scheme 1 illustrates the production of the 3D sponge-like GO material from disperse GO flakes. Mixing of the aqueous GO suspension with ascorbic acid under mild thermal and pressure conditions produces the 3D material which is characteristic of an ultra-light weight sponge. The scheme then illustrates the preparation of the Fe impregnated rGO, either as flakes or sponge structure, using the polymeric resin/citrate complex, via a single combined impregnation and thermal reduction step. The Fe-rGO flakes and sponge are subject to an impregnation process by the iron salt precursor to obtain the appropriate functionalized material, wherein the salt chemistry and impregnation concentration can be easily varied.

SEM and HRTEM images (Figure 1) give examples of several large nanocrystals possessing a distinct core-shell structure. The number of nanocrystals contained within the GO sheet is dependent upon the concentration of the original polymeric resin, and as such allows the synthesis of Fe-rGO materials containing high or low concentrations of nanoparticles (Figures 1A and 1B, respectively), although unattached nanoparticles were observed in samples prepared using a high concentration of Fe salts. The integrated nanoparticles were characterized via EDX and EELS, which confirmed the presence of metallic Fe and iron oxide within these core-shell structures. The Fe nanoparticles are synthesized during the calcining step, where the pyrolysis of the polymeric solution creates a CO/CO_2 atmosphere within the furnace. This, in turn, reduces the Fe (III) nitrate within the GO matrix, obviating the need for hydrogen as a reducing agent [11].

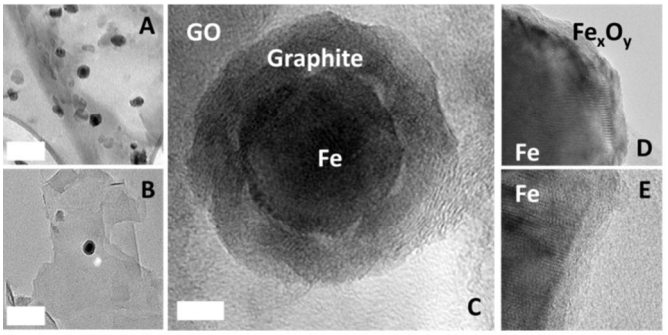

Figure 1. (A and B) TEM (bars = 50 nm) and (C) STEM (bar = 5 nm) images of GO functionalized with core-shell Fe-graphite nanoparticles, and (D and E) EELS images showing the oxide layer on the FE nanoparticles.

The observation of the ensemble of Fe nanoparticles on the GO flakes suggest in particular that the organic resin on the Fe salt suspension deposits a residual carbon layer during the thermal treatment (from the decomposition step of the citrate-polymeric complex). This helps in dispersing the Fe nanoparticles and assists in their attachment to the GO flakes. A similar observation has been made previously for carbon encapsulated nickel and Fe nanoparticles respectively [20]. However, the carbon encapsulated Fe nanoparticles in the previously reported case [20] did not favor the formation of magnetic nanoparticles due to the oxidation of the Fe by water during the reaction (the encapsulated magnetic nanoparticles were developed by heating in an aqueous glucose solution). This suggests that parameters including the chemical synthesis method, the solvent, the functional groups on the solvated coordination complex, the polymerization step and the thermal treatment can lead to significant surface modifications on the encapsulated nanoparticles [18, 20-21], and therefore must be carefully controlled.

The Fe-rGO sponge structures are illustrated in Figure 2, with an example of (A) the pristine sponge and (B) the nanoparticle decorated analogue, wherein the large surface are of the sponge materials could be useful in adsorption processes.

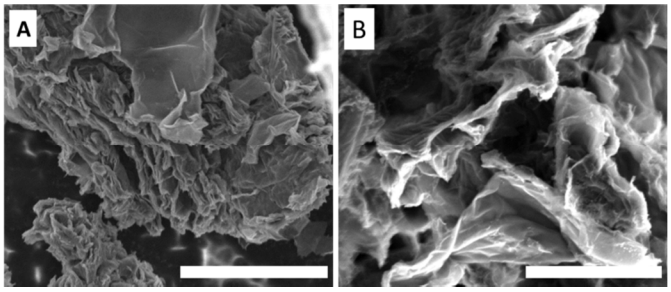

Figure 2. SEM images of (A) pristine GO sponge material (bar = 10 µm), and (B) the Fe nanoparticle decorated analogue (bar = 5 µm).

An ultrathin carbonaceous shell can be observed surrounding each Fe nanoparticle (Figure 1), and frequently this is associated with a thin iron oxide coating around the Fe nanoparticles. The residual carbon could have potential material advantages, including metal stability, non-toxicity, and enhanced integration of the Fe phase with the rGO surface [20, 22]. In order to investigate the interface of the Fe-carbon shell and the GO surface, complementary EDAX (Energy-dispersive X-ray spectroscopy) analysis was undertaken. Figure 3 shows the XRD pattern for GO, rGO and the Fe-rGO sponge (13.5 wt. % Fe). The XRD pattern shows the typical metallic Fe and iron oxide crystalline phases, respectively, present in the hybrid composite structure.

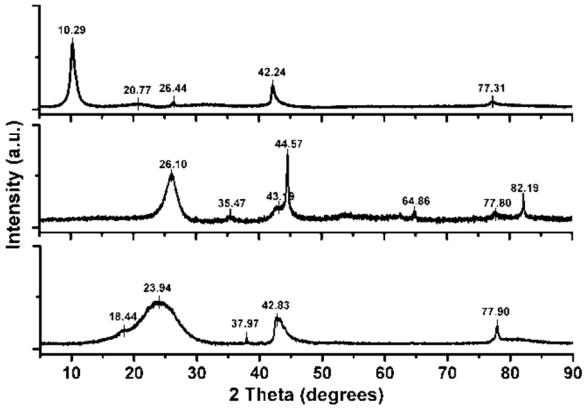

Figure 3. XRD spectra of (top) GO, (middle) Fe-rGO and (bottom) rGO.

The major peaks present in GO at 10.29°, 42.24°, and 77.31° closely match those expected for graphene oxide [23]. Similarly, the major peaks present in rGO at 23.94°, 42.83°, and 77.90°, are similar to expected values for rGO [23]. By using the peak at 10.29°, the interlayer spacing of GO is calculated to be 8.8 Å, while the peak at 23.94° for rGO shows the interlayer spacing for rGO to be 3.7 Å. This decrease in interlayer spacing is expected and is due to the removal of oxygen and water from between the layers of carbon [24].

The peaks present in Fe-rGO at 26.10°, 43.19° and 77.80° correspond to the rGO in the sample. In this case, the interlayer spacing is calculated to be 3.4 Å. The peaks present at 44.57°, 64.86°, and 82.19° are due to the presence of metallic Fe in the sample. The remaining peak, present at 35.47°, could be indicative of a small amount of iron oxide, either in the form of magnetite or maghemite. It is therefore theorised that the Fe nanoparticle produced has a metallic Fe core with a thin shell of iron oxide, which is then coated in rGO. By analysing the 44.57° peak, with the help of the Scherrer formula [25], the average diameter of the metallic Fe core in the nanoparticles can be estimated as 24.8 nm. This estimation seems to be consistent with the dimensions of the nanoparticles shown in figure 1.

Specific surface area measurements give the surface areas of the graphite and the Fe-rGO sponge materials (3.2 and 13.5 wt. % Fe), resulting in 4.11, 92.82, 66.62 m^2/g, respectively. The specific surface area of the Fe-rGO is somewhat lower than that for other typical carbon frameworks [26] due to the thermal treatment of the sponges which causes them to become compacted but well protected from its environment. The presence of the nanoparticles and any traces of residual raw materials (such as ascorbic acid) may also have the effect of reducing the specific surface area.

During the preparation of the Fe-rGO sponge, increasing the concentration of Fe salt in the preliminary complex solution (**B** in scheme 1) directly reflects on the thermal stability of the composite and its subsequent dimensions. The production of the complex, and subsequent single thermal treatment step, allows for a degree of control of the concentration of nanoparticles on the surface of the rGO sheets. For example, Fe-rGO sponges with different dimensions, produced using 1.1, 3.2, and 13.5 wt. % Fe respectively, are illustrated in Figure 4, suggesting that a compromise needs to be achieved between the nanoparticle loading and the sponge's physical properties depending on the required application.

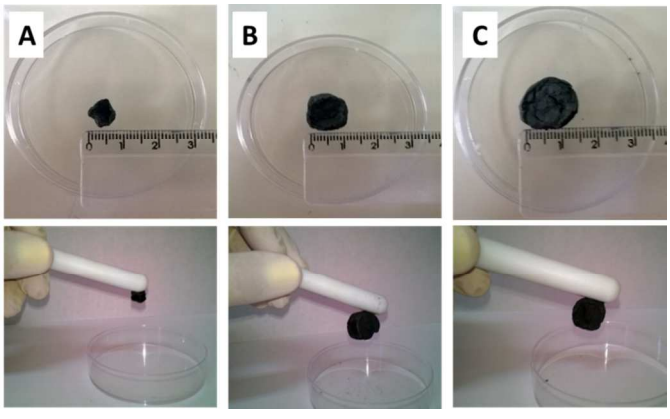

Figure 4. Fe-rGO sponges produced using increasing concentrations of Fe nanoparticles: (A) 1.1, (B) 3.2, and (C) 13.5 wt. % Fe respectively.

Aside from reducing the graphene oxide, and restoring the electronic conjugation in the molecule, the ascorbic acid may promote cross-linking between graphene oxide sheets in a

manner similar to that found for sol-gel prepared graphene aerogels [19, 27]. In the sol-gel formation, the hydrogelation gradually promotes overlap and restores the strong π–π interactions between the rGO sheets: a similar mechanism may occur in the production of the sponges produced here. The use of ascorbic acid also has the advantage that no gaseous products are formed during the sponge formation. Frequently used reducing agents, such as hydrazine, NaBH4, LiAIH4, etc., can evolve gaseous products which consequently produce non-uniform structures. [19, 27] The insertion of the Fe nanoparticles, by impregnation of the Fe- resin and subsequent annealing, promotes additional surface modification via the functional groups on the metal-citrate complex, and reinforces the 3D matrix.

The magnetic hysteresis loop measured for the hybrid Fe-rGO flakes with different Fe concentrations is shown in figure 5. Typical ferromagnetic behavior [28] is observed for all samples, although the magnetic hysteresis curves show a significant shift on the horizontal axis. Such a shift is usually observed in core shell Fe nanoparticles covered with a Fe_2O_3 shell due to an exchange-bias field generated by inter-particle magnetic interactions [29]. A coercivity field (H_C) of 216 and 98 kG is estimated for 3.2 and 13.5 wt. % Fe nanoparticle samples respectively. The magnitude of H_C could be related to the thickness of the shell oxide layer, which changes with an increase in the quantity of Fe. Subsequently, we confirmed, by a study of the temperature dependence of the magnetization on 5 wt. % Fe containing rGO samples, that a thin oxide surface layer can be formed (Figure 1D), leading to a core shell morphology where an antiferromagnetic (AFM) oxide layer surrounds the ferromagnetic (FM) metallic Fe nanoparticle. Such morphology influences the magnetic properties due to the exchange interaction between the FM and AFM phases [30].

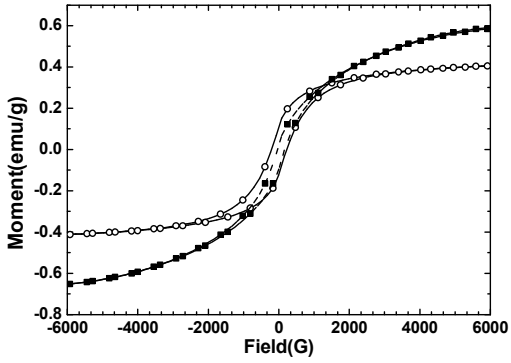

Figure 5. Room temperature magnetic hysteresis loops measured for the hybrid Fe-rGO flakes with different Fe concentrations: (○) 3.2, and (■) 13.5 wt. % Fe.

The magnetic properties of the Fe-rGO materials were demonstrated by bringing a dispersed sample into close proximity with a permanent magnet. This resulted in an immediate attraction between the Fe-rGO and the magnet which is strong enough to draw the flakes out of suspension. The strength of this attraction was such that it was possible to drag the vial across the floor of the fume cupboard without breaking the connection between the Fe-rGO and the magnet.

3.2 Dye removal from aqueous solution

The scheme in Figure 6 illustrates the efficiency of the Fe-rGO sponge (7 mg) in removing Rhodamine B (Rho B) from aqueous solution (2 x 10^{-7} mol/L). Rho B is a textile dye that can potentially be harmful to the environment if released into water courses, and has been found to be toxic [31]. UV-visible spectroscopy analysis after immersion for 24 h. (Figure 6E) shows that the magnetic sponge has the capacity to remove significant quantities of the dye from aqueous solution in a safe and compact manner. Using Figure 6E, the selective removal of dye was determined to be 2.59 x 10^{-5} mol/g, a value consistent with similar results for carbon materials [32]. Accordingly, the complete removal of the dye is expected to occur after approx. 30 h.

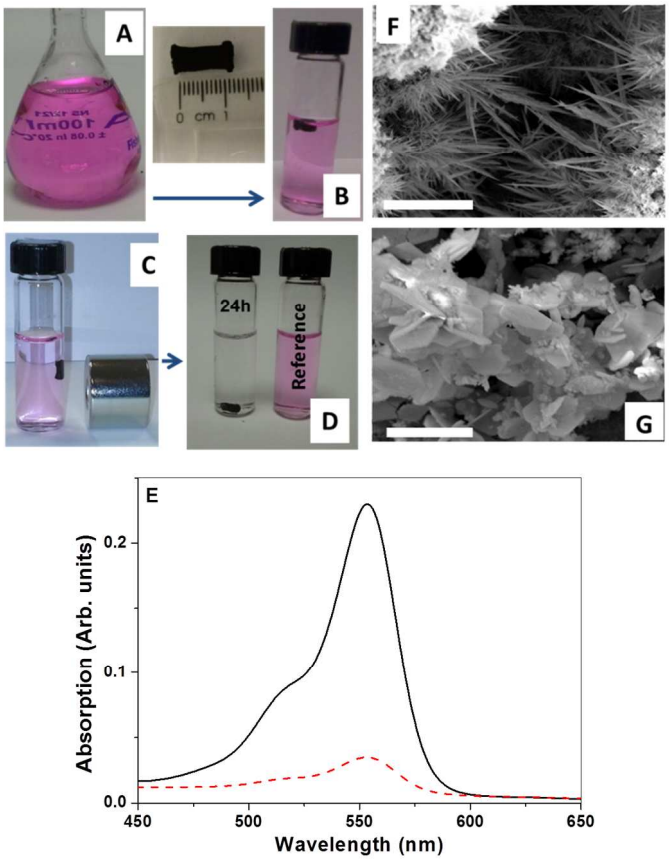

Figure 6. Take up of Rhodamine B from aqueous solution (2x10^{-7}mol/L) and subsequent retrieval of the Rho B using ethanol. The Rhodamine solution (A) is absorbed by the magnetic GO-sponge (B and C), and is removed from solution within 24 h. (D). UV-visible spectra of the remaining solution (E) shows the reduction in Rho B concentration, before (solid line) and after (dashed line) Rho B absorption, and SEM images (F and G) show the formation of Rho B crystals in the 3D Fe-rGO sponge matrix (bars = 20 and 5 µm respectively).

Previous work describes the characteristic forces producing the aggregation and precipitation of the dye crystals on the Fe-rGO flake surface (Figure 6F and G). The affinity of materials to

adsorb molecules is mainly determined by H-bonding, van der Waals, π–π and electrostatic interactions [26, 33, 34]. Through these mechanisms, the Rho B nucleates on the surface of the GO matrix and crystallizes. Fe-rGO flakes also tend to aggregate in water due to Van der Waals interactions between neighbouring sheets causing a reduction in the surface area which is not beneficial for the adsorption of contaminants. This is overcome to some extent using the 3D GO sponge.

The Rho B may be eluted from the Fe-rGO sponge matrix, with the consequent recovery of the sponge, by immersion in ethanol (Figure 7), which has a higher affinity for the Rho B molecules. Figure 7C illustrates the Rho B desorption performance of Fe-rGO and GO sponges 24 and 216 h. after absorption, where the contaminant dye is recovered from the sponges using ethanol. The recovery of the Rho B from the sponges is an important feature of contaminant recovery, and indicates that potentially valuable pollutants can be safely extracted and recovered, and that the sponges can be reused. However, after 216 h., independent of the nature of the sponge composite, the ability to recover the Rho B is significantly reduced using an ethanol wash alone. It is assumed that the pores in the sponges are blocked by fully crystallized Rho B crystals which do not allow the ethanol to fully enter the carbon matrix. This can be resolved by immersion of the Rho B loaded sponge in ethanol (or a mixture of compatible organic solvents) that is heated to approx. 60 °C.

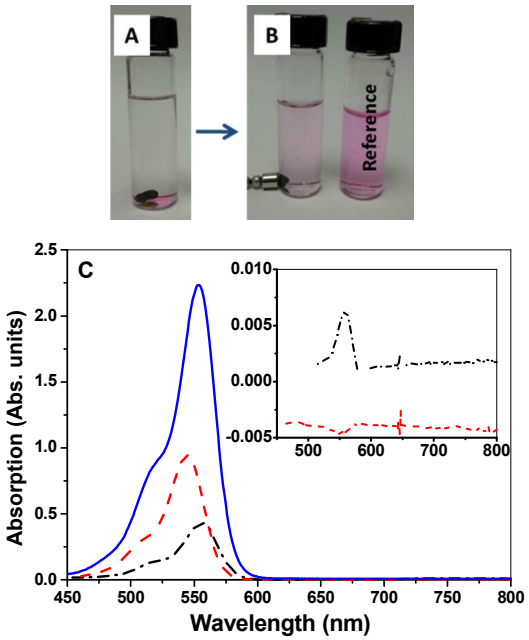

Figure 7. Recovery of absorbed Rho B, and regeneration of the sponge, by elution with ethanol: after (A) 5 s, and (B) 2 min. (C) UV-visible spectra of the Rho B reference is given (solid line), with Rho B solution desorbed from Fe-rGO (dash-dot line) and GO sponge matrices (dashed line) after 24 and (inset) after 216 h respectively.

Figure 8 shows a Fe-rGO sponge acting on a methylene blue spill (0.01 mol/L) (A-C), and absorption from solution (D-E), with similar results. It is not thought that the iron nanoparticles assist in the absorption of the dye molecules as nanoparticle-free rGO sponges are also seen to absorb dye, however the nanoparticles add magnetic functionality, broadening the applicability of the sponge materials.

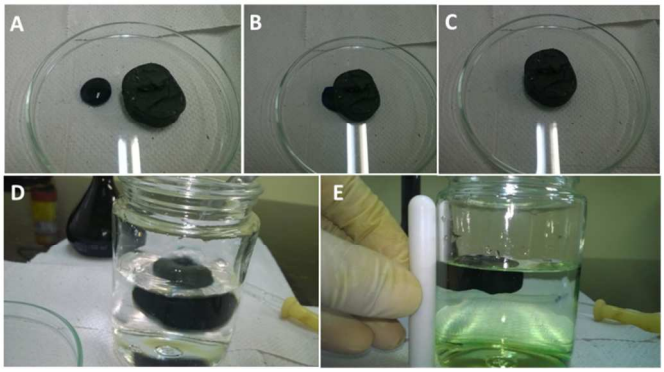

Figure 8. (A-C) Fe-rGO sponge adsorption of methylene blue (0.01 mol/L), after (B) 2s and (C) complete adsorption after 10s, (D and E) Removal of the dye from aqueous solution.

3.3 XPS analysis

3.3.1 Graphene oxide peak fitting

XPS analysis over the range of the C1s binding energies (Figure 9A) gives rise to multiple peaks, indicative of the various bonding states of the carbon, and can be split in to four components: (1) a small shoulder at 283.5 eV, attributed to a small amount of C-H bonds present in the sample; (2) a peak at 284.9 eV, attributed to non-oxygenated sp^2 carbon, reflecting the amount of graphitic material in the sample that has not been oxidized; (3) singly bonded carbon-oxygen groups (C-O) at 286.9 eV; and (4) the carboxylate carbon (O-C=O) at 288.6 eV.

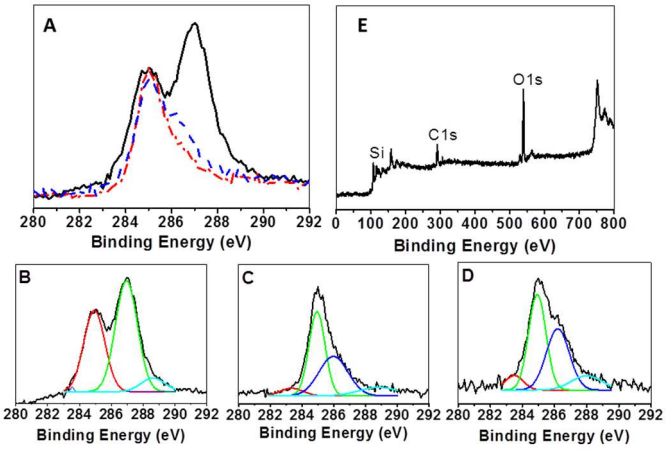

Figure 9. (A) High resolution XPS spectra of GO (solid line), rGO (dashed line) and Fe-rGO (3.2 wt. % Fe) (dash-dot line), where the major peaks at 284.9 and 286.9 eV have been ascribed to non-oxygenated (graphitic) sp^2 carbon and singly bonded carbon-oxygen (C-O) groups respectively. (B-D) Deconvoluted spectra of GO, rGO and Fe-rGO respectively, where the plots correspond to the full spectrum (black line), and deconvolution plots corresponding to C-C (red), sp^2 carbon (green), C-O (blue), and O-C=O (cyan). (E) is a wide spectrum XPS scan of Fe-rGO (3.2 wt. % Fe).

3.3.2 Reduced Graphene Oxide peak fitting

As confirmed by XPS, the GO (Figure 9B) is chemically reduced to obtain rGO (Figure 9C), with a much smaller quantity of oxygen present in the system. The amount of carbon present bonded to oxygen (in C–O single bonds, C=O carbonyl bonds, and –COO– carboxylic groups) has been dramatically reduced in the rGO during thermal treatment, with the majority of carbon now present as C=C sp^2 bonds (285 eV peak), consistent with the presence of graphitic carbon allotropes. However, the presence of a significant C-O peak (286 eV peak) reveals that some oxygen containing groups are still present within the sample.

The profile of the C1s peak in Fe-rGO (Figure 9D) looks very similar to that of rGO. However, the shoulder of the C-O peak (at 286.2 eV) appears to be more identifiable [35, 36]. This difference is quite small and probably a result of variation across the sample rather than a different chemical oxidation environment as a result of the Fe functionalization. A wide spectrum XPS scan of the Fe-rGO (Figure 9E) confirms a lack of Fe species (oxides or reduced Fe) indicative of surface decoration of the carbon [37, 38]. Furthermore, the larger shoulder at the lower binding energy side of the peak may hint at the presence of slightly more amorphous carbon [39, 40], which would be a result of the Fe decoration if all of the added carbon was not graphitized. These observations are in agreement with carbon encapsulated Fe clusters rather than a carbon surface decorated with exposed Fe.

3.4 H_2-TPR for Fe-rGO samples

In order to obtain additional detail on the role of the carbon layer on the metal nanoparticles, TPR studies were completed. Figure 10 shows the H_2 consumption due to reduction of iron oxide, where the H_2 consumption band observed at 400 °C is related to partial reduction of iron oxide (hematite) and the formation of magnetite (Fe_3O_4). The second band of H_2 consumption (between 450 and 600 °C) is related to the reduction of magnetite to form iron oxide (FeO). The third band (>600 °C) is attributed to reduction of FeO to Fe(0) [41]. However, due to the relative H_2 consumption, it is comprehensible that some Fe(0) is formed in the range 450 to 600 °C.

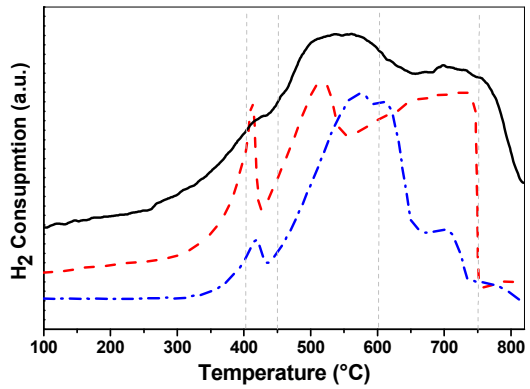

Figure 10. H_2-TPR plots for Fe-rGO with increasing concentrations of Fe: 1 (solid line), 10 (dashed line), and 35 (dash-dot line) wt. % Fe respectively. The dashed vertical lines act as a guide to the relevant temperature ranges.

The intensity of the initial peak, at approx. 400 °C, depends on the carbon coverage of the integrated Fe_2O_3 particles. The sample containing 1 wt. % Fe displays only a small shoulder at 400 °C, attributed to a comprehensive coverage of the Fe_2O_3 particles by the carbon coating. Increasing amount of Fe, to 10 wt. % Fe, produces a more defined H_2 consumption peak at 400 °C. This suggests that the fraction of iron oxide particles that are not fully coated with a carbon layer is higher, which may be due to an increasing iron oxide particle size. The relatively low H_2 consumption peak at 400 °C for the 35 wt. % Fe sample suggests that larger iron oxide particles are formed in the higher concentration samples, producing a lower oxide surface area, and hence lower surface reactivity at this low temperature, when compared to the 10 wt. % Fe sample.

The majority of the reduction of Fe_2O_3 to FeO is observed in the second temperature band between 450 and 600 °C, before complete reduction to FeO above 600 °C. Note that in the high Fe content (35 wt. %) sample the location of the second H_2 consumption peak (at 570 °C) is shifted as the larger nanoparticles require more heating before becoming susceptible to reduction throughout the nanoparticle. Finally, in the 10 wt. % Fe sample, H_2 consumption ceases abruptly at 750 °C as all the Fe is reduced. This effect is also observed to varying extents in the 1 and 35 wt. % Fe samples, in the temperature range between 650 and 800 °C, but is less pronounced.

The carbon coated particles naturally present a higher resistance to the reduction process at low temperatures, and consequently the reduction occurs slowly. The amount of iron oxide in the 35 wt. % Fe sample is much higher, consequently the particle diameter is higher, and given the same amount of rGO is used in each sample, the fraction of Fe coated by carbon is consequently lower. However, the larger dimensions of the nanoparticles in the 35 wt. % Fe sample means that they require more heat to be fully reduced.

According to the thermogravimetry observations, the thermal stability of the sponge is found to increase with Fe concentration. This consequently leads to a significant improvement in the stability of the larger sponges. However, it is unlikely that this process is linear in nature as, depending on the method of incorporation and the effective impregnation of the Fe-polymeric resin, large concentrations of Fe can lead to large amounts of unprotected and unbound Fe on the GO surface which will ultimately collapse the sponge. The challenge is to avoid sponge collapse while incorporating adequate concentrations of metal nanoparticles over a large surface area suitable for the subsequent application.

3.5 Integration into PDMS

An alternative composite system was prepared using PDMS. PDMS was chosen as a polymer matrix for its many desirable characteristics, including good thermal and oxidative stability, low glass transition temperature, low surface free energy, low

toxicity, hydrophobic surfaces, and low chemical reactivity [42]. Films were produced by solution casting PDMS, during which the material could be easily modified through the introduction of Fe-rGO nanoparticles. Figure 11A shows the pure and modified PDMS polymer matrix, while Figure 11B gives the magnetic hysteresis loop measured for Fe-rGO in the PDMS.

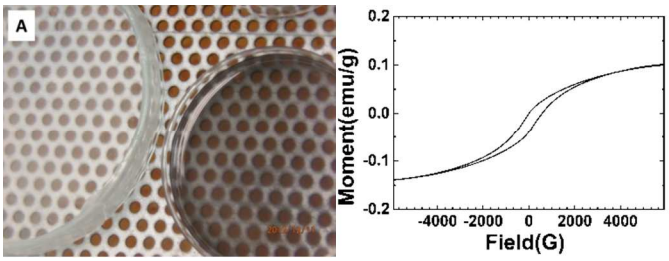

Figure 11. (A) Images of pristine PDMS and Fe-rGO modified PDMS films, and (B) the magnetic hysteresis loop for Fe-rGO modified PDMS.

A PDMS sample without incorporated magnetic nanoparticles returned no signal when subjected to magnetic hysteresis measurements. The magnetic behaviour is therefore ascribed to the Fe nanoparticles deposited on the rGO and integrated into the PDMS polymeric membrane, and is analogous to magnetic properties observed for PDMS dispersed Fe nanoparticles. [4] The physical and magnetic properties of the PDMS composite can be altered depending on the PDMS composition and dimensions, and the Fe-rGO loading.

The polymer nanocomposite has potential in coating applications requiring flexible and functional surfaces, or in the removal of contaminants from gaseous environments given the gas permeability of PDMS, while the embedded Fe-rGO nanoparticles retain their magnetic characteristics. A graphene functionalized PDMS material with super-hydrophobic and super-oleophilic properties has been produced and has been used for the separation and absorption of oils or organic solvents from water. [39] A similar application may be found for the Fe-rGO/PDMS materials produced here, where the Fe-rGO can be used to manipulate beads of PDMS.

Conclusions

The hybrid carbon magnetic materials described here, derived from rGO flakes functionalized with Fe particles, show promise for environmental applications. The 2D and 3D rGO materials are functionalized by organic/inorganic core shell nanoparticles during the thermo-chemical processing of the precursor solution. The resultant morphological, magnetic and surface analysis helps to explain the physico-chemical behaviour of the materials and points the way to potential applications in, amongst others, water treatment, such as for the removal of industrial dyes.

In this case, the nanoparticles are primarily included in the carbon matrix to aid in the post absorption clean-up of contaminants. The carbon sponge material can be distributed in an area of contaminated watercourse and allowed to absorb the contaminants. After this, the sponge material can be efficiently collected from the watercourse by magnetic means. Certain contaminants (such as the dyes used here) can be removed (by using a solvent with a higher affinity for the carbon in this case) and the magnetic sponge materials reused.

The dimensions/volume of the sponge depends on the application. For the decontamination of water courses, the volume of the sponge depends on the optimal dimensions for manipulation. Most likely, this will be a powdered or pellet form which can be easily transported, scattered and then collected using the magnetic functionality of the sponge. In an alternative example, cylindrical activated carbon briquettes are commonly used in domestic water filtration apparatus.

The dimensions of the sponges produced here are defined by the vessels in which they are produced, and it is envisaged that the production process is scalable to larger dimensions. Given suitable sponge dimensional stability, tubular briquettes may be produced that can be mechanically cut to smaller sizes, or individual briquettes may be formed of different dimensions by choosing the appropriate reaction vessel.

The composite material has been shown to exploit the advantageous properties of both the high surface area carbon network, with specific surface areas greater than 50 m^2/g, and the ferromagnetic iron nanoparticles, with coercivity fields of 100 kG or better typical for ferrite magnets. The use of carbon materials also opens the hybrid materials to further chemical functionalization or co-decoration, with silver nanoparticles for example, for enhanced chemical uptake of contaminants or bactericidal properties respectively. Investigations into the effects of heating under standard atmosphere and in the presence of aggressive chemicals are ongoing in order to determine the scope and role of the core graphite layer as a protective material, with promising preliminary results.

Acknowledgements

The authors are grateful to the Brazilian National Council for Scientific and Technological Development for financial support through CNPq and CAPES (# 9766-11-1).

Notes and references

[a] Materials Engineering, Technology Development Center, Federal University of Pelotas, Pelotas, RS, CEP 96010-610, Brazil.
[b] Federal University ABC, São Bernardo do Campo, SP, CEP 09210-580, Brazil.
[c] Federal University Ceará, CEP 60455760 - Fortaleza, CE, Brazil.
[d] Nano-Electronics Centre, Advanced Technology Institute, University of Surrey, Guildford, GU2 7XH, UK.
[e] Advanced Coatings Group, Surface Engineering Department, Tata Steel Research Development and Technology, Swinden Technology Centre, Rotherham, S60 3AR, UK.

1 http://www.eoearth.org/view/article/162358/
2 K. Kawata, H. Yokoo, R. Shimazaki and S. Shiokabe, *Environ. Sci. Technol.*, 2007, **41**, 3769.

3 F. Aguilera, J. Méndez, E. Pásaro and B. Laffon, *J. Appl. Toxicol.*, 2010, **30**, 291.
4 C. Wu, X. Huang, X. Wu, R. Qian and P. Jiang, *Adv. Mater.*, 2013, **25**, 39.
5 Y. Zhu, S. Murali, W. Cai, X. Li, J. W. Suk, J. R. Potts, and R. S. Ruoff, *Adv. Mater.* 2010, **22**, 3906.
6 Y. Su, V. G. Kravets, S. L. Wong, J. Waters, A. K. Geim, and R. R. Nair, 2014, *Nature Commun.* 2014, **5**, 4843.
7 N. Shang, P. Papakonstantinou, P. Wang, and S. R. P. Silva, *J. Phys. Chem. C,* 2010, **114**, 15837.
8 C. T. G. Smith, R. W. Rhodes, M. J. Beliatis, K. D. G. I. Jayawardena, L. J. Rozanski, C. A. Mills, and S. R. P. Silva, *Appl. Phys. Lett.,* 2014, **105**, 073304.
9 M. J. Beliatis, K. Gandhi, L. J. Rozanski, R. Rhodes, L. McCafferty, M. R. Alenezi, A. S. Alshammari, C. A. Mills, K. D. G. I. Jayawardena, S. J. Henley, and S. R. P. Silva, *Adv. Mater.,* 2014, **26**, 2078.
10 S. Shi, V. Sadhu, R. Moubah, G. Schmerber, Q. Bao, and S. R. P. Silva *J. Mater. Chem. C*, 2013, **1**, 1708.
11 H. Bi, X. Xie, K. Yin, Y. Zhou, S. Wan, L. He, F. Xu, F. Banhart, L. Sun and R.S. Ruoff, *Adv. Func. Mater.*, 2012, 22, 4421.
12 G. Zhao, J. Li, X. Ren, C. Chen and X. Wang, *Environ. Sci. Technol.*, 2011, **45**, 10454.
13 F. Guo, G. Silverberg, S. Bowers, S-P. Kim, D. Datta, V. Shenoy and R.H. Hurt, *Environ. Sci. Technol*., 2012, **46**, 7717.
14 H. Bi, Z. Yin, X. Cao, X. Xie, C. Tan, X. Huang, B. Chen, F. Chen, Q. Yang, X. Bu, X. Lu, L. Sun and H. Zhang, *Adv. Mater.*, 2013, **25**, 40.
15 H. Wang, X. Yuan, Y. Wu, H. Huang, X. Peng, G. Zeng, H. Zhong, J. Liang and M. Ren, *Adv. Coll. Interf. Sci.*, 2013, **19**, 195.
16 W. S. Hummers and R. E. Offeman, *J. Amer. Chem. Soc.*, 1958, **80**, 1339.
17 L. McCafferty, V. Stolojan, S. G. King, W. Zhang, S. Haq, and S. R. P. Silva, *Carbon* 2015, **84**, 47.
18 E. R. Leite, N. L. V. Carreno, E. Longo, F. M. Pontes, A. Barison, A. G. Ferreira, Y. Maniette and J. A. Varela, *Chem. Mater.*, 2002, **14**, 3722.
19 X. Zhang, Z. Sui, B. Xu, S. Yue, Y. Luo, W. Zhan and B. Liu, *J. Mater. Chem.*, 2011, **21**, 6494.
20 Z. Wang, P. Xiao and N. He, *Carbon*, 2006, **44**, 3277.
21 X. M. Sun and Y. D. Li, *Angew. Chem. Int. Ed.*, 2004, **43**, 597.
22 J. Huo, H. Song and X. Chen, *Carbon*, 2004, **42**, 3177.
23 H. Feng, R. Cheng, X. Zhao, X. Duan and J. Li, *Nature Commun.*, 2013, **4**, 1539.
24 S. H. Huh, in Thermal Reduction of Graphene Oxide, ed. S. Mikhailov, InTech, 2011, ch. 5, pp. 73-91.
25 A. Patterson, *Phys. Rev.*, 1939, **56**, 978.
26 J. Zhao, W. Ren and H-M. Cheng, *J. Mater. Chem.*, 2012, **22**, 20197
27 J. Zhang, H. Yang, G. Shen, P. Cheng, J. Zhang and S. Guo, *Chem. Commun.*, 2010, **46**, 1112.
28 D. L. Huber, *Small*, 2005, **1**, 482-501.
29 R. K. Zheng, G. H. Wen, K. K. Fung and X. X. Zhang, *J. Appl. Phys.*, 2004, **95**, 5244.
30 F. C. Fonseca, G. F. Goya, R. F. Jardim, N.L.V. Carreño, E. Longo, E. R. Leite and R. Muccillo, *Appl. Phys. A*, 2003, **76**, 621.
31 T. A. Khan, I. Ali, V. V. Singh and S. Sharma, *J. Environ. Prot. Sci.*, 2009, **3**, 11.
32 S. Wang and H. Li, *J. Hazard. Mater.*, 2005, **B126**, 71.
33 S. J. Zhang, T. Shao, S. S. K. Bekaroglu and T. Karanfil, *Environ. Sci. Tech.,* 2009, **43**, 5719.
34 G. K. Ramesha, A. V. Kumara, H. B. Muralidhara and S. Sampath, *J. Coll. Interf. Sci.*, 2011, **361**, 270.
35 W. Chen, L. Yan and P. R. Bangal, *Carbon*, 2010, **48**, 1146.
36 D. R. Dreyer, S. Park, C, W. Bielawski and R. S. Ruof, *Chem. Soc. Rev.*, 2010, **39**, 228.
37 X. Yang, C. Chen, J. Li, G. Zhao, X. Ren and X. Wang, *Roy. Soc. Chem. Adv.*, 2012, **2**, 8821.
38 S. Steiner, T. F. Baumann, J. Kong, J. H. Satcher and M. S. Dresselhaus, *Langmuir*, 2007, **23**, 5161.
39 J. Filik, P. W. May, S. R. J. Pearce, R. K. Wild and K. R. Hallam, *Diamond Relat. Mater.*, 2003, **12**, 974.
40 Y. Yun, E. Broitman and A. J. Gellman, *Langmuir*, 2010, **26**, 908.
41 T. P. Braga, B. M. C. Sales, A. N. Pinheiro, W. T. Herrera, E. Baggio-Saitovitch and A. Valentini, *Catal. Sci. Technol.*, 2011, **1**, 1383.
42 D. D. Nguyen, N.-H. Tai, S. B. Lee and W. S. Kuo, *Energy Environ. Sci.*, 2012, **5**, 7908.